

Electronic Supplementary Material (ESI)

Synthesis, fabrication and characterization of 2-naphthyloxy group-substituted bis(2-pyridylimino)isoindoline and its derivatives as positive electrode for vanadium redox flow battery applications

Selin Gümrukçü^a, Mukaddes Özçeşmeci^a, Nilüfer Koçyiğit^b, Kerem Kaya^a, Ahmet Gül^a,
Yücel Şahin^{c*}, İbrahim Özçeşmeci^{a*}

^aIstanbul Technical University, Department of Chemistry, TR-34469, Maslak, Istanbul,
Turkey

^bBiruni University, Department of Basic Pharmaceutical Sciences, Faculty of Pharmacy,
TR34010, Istanbul, Turkey

^cYıldız Technical University, Faculty of Arts & Sciences, Department of Chemistry, TR34220
Istanbul, Turkey

Table of Contents

Figure S1. FT-IR spectrum of **BPI** and **PdBPI**.

Figure S2. UV-vis spectra of **BPI** and **PdBPI** in DMF (5×10^{-5} M).

Figure S3. ^1H -NMR spectrum of **BPI** in CDCl_3 .

Figure S4. ^{13}C -NMR spectrum of **BPI** in CDCl_3

Figure S5. ^1H -NMR spectrum of **PdBPI** in CDCl_3 .

Figure S6. ^{13}C -NMR spectrum of **PdBPI** in CDCl_3 .

Figure S7. MALDI TOFF MS spectrum of **BPI**.

Figure S8. MALDI TOFF MS spectrum of **PdBPI**.

Figure S9. SEM images of PGE/BPI (a) and PGE/PdBPI (c), and EDX elemental mapping results of PGE/BPI (b) and PGE/PdBPI (d).

Figure S10. XPS Survey spectra of BPI-CF (a) and PdBPI-CF (b).

Figure S11. Electrochemical stability test of **PGE/BPI**.

Figure S12. Electrochemical stability test of **PGE/PdBPI**.

Table S1. Structure refinement parameters of **BPI** and **PdBPI**.

Table S2. Selected bond lengths (\AA) **BPI** and **PdBPI**.

Table S3. Selected bond angles ($^\circ$) **BPI** and **PdBPI**.

Table S4. Comparison of CE, EE and VE based on previous reported studies.

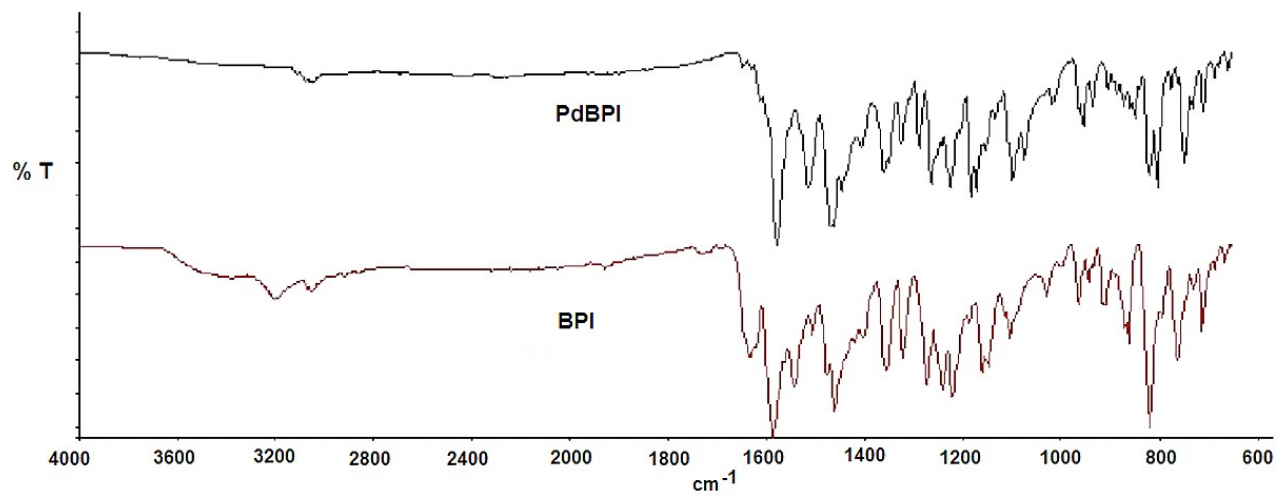


Figure S1. FT-IR spectrum of **BPI** and **PdBPI**.

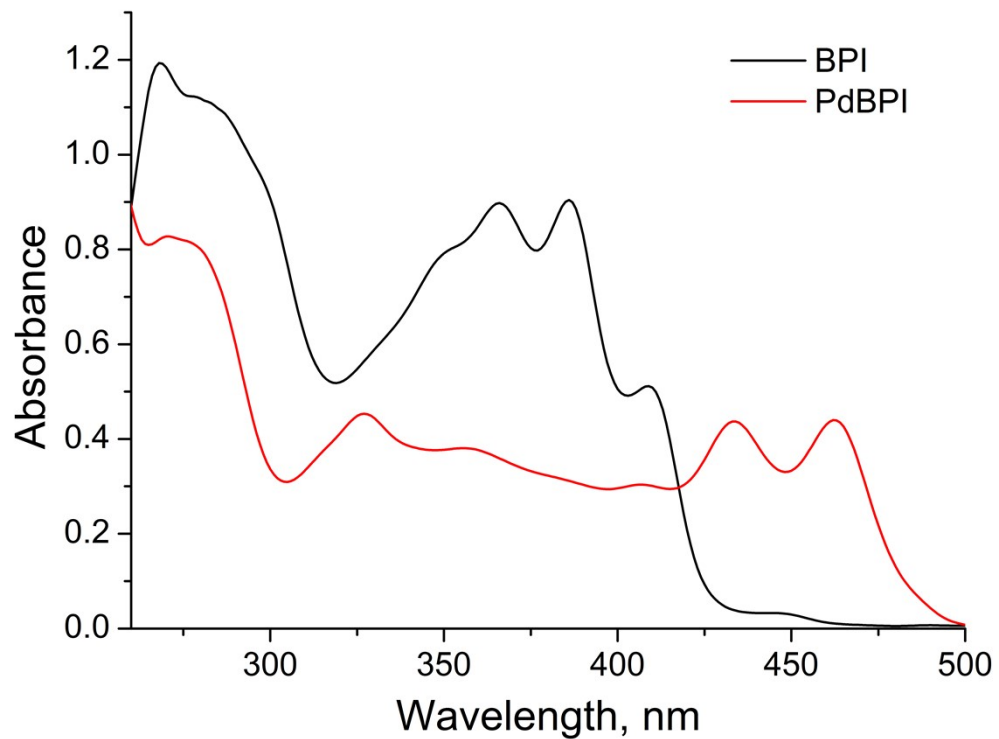


Figure S2. UV-vis spectra of **BPI** and **PdBPI** in DMF (5×10^{-5} M).

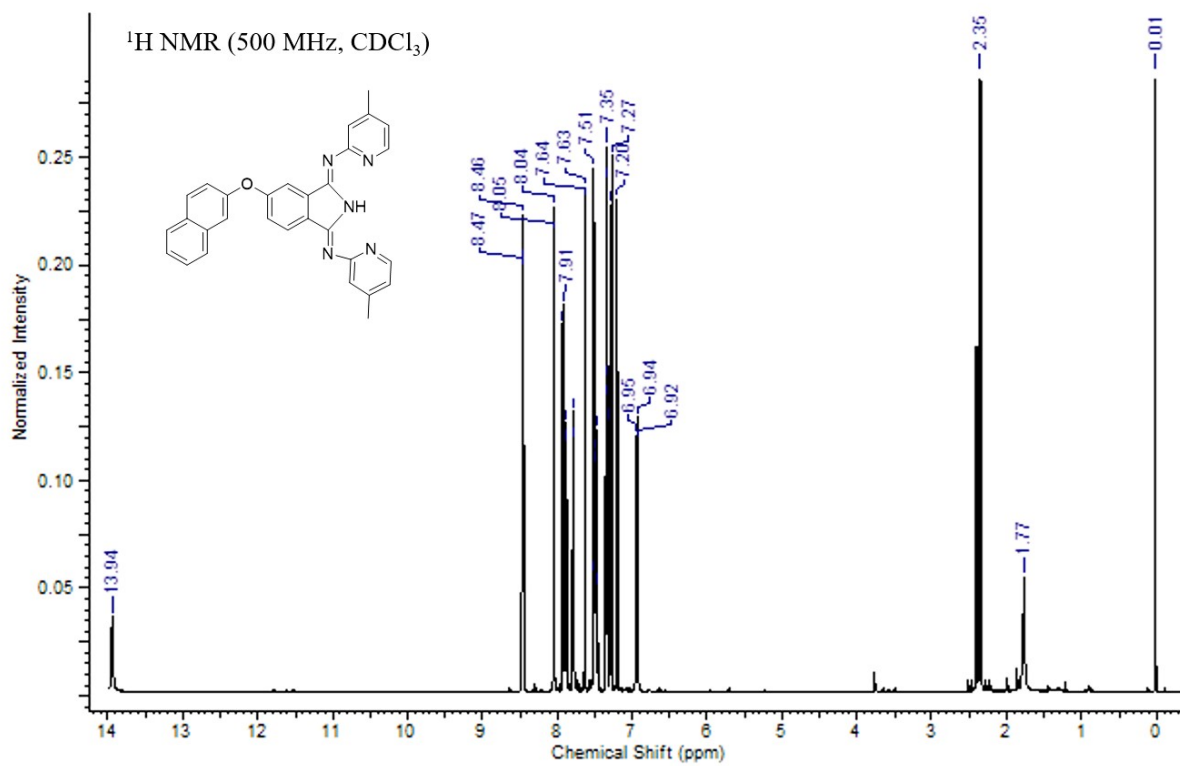


Figure S3. ¹H-NMR spectrum of BPI in CDCl₃.

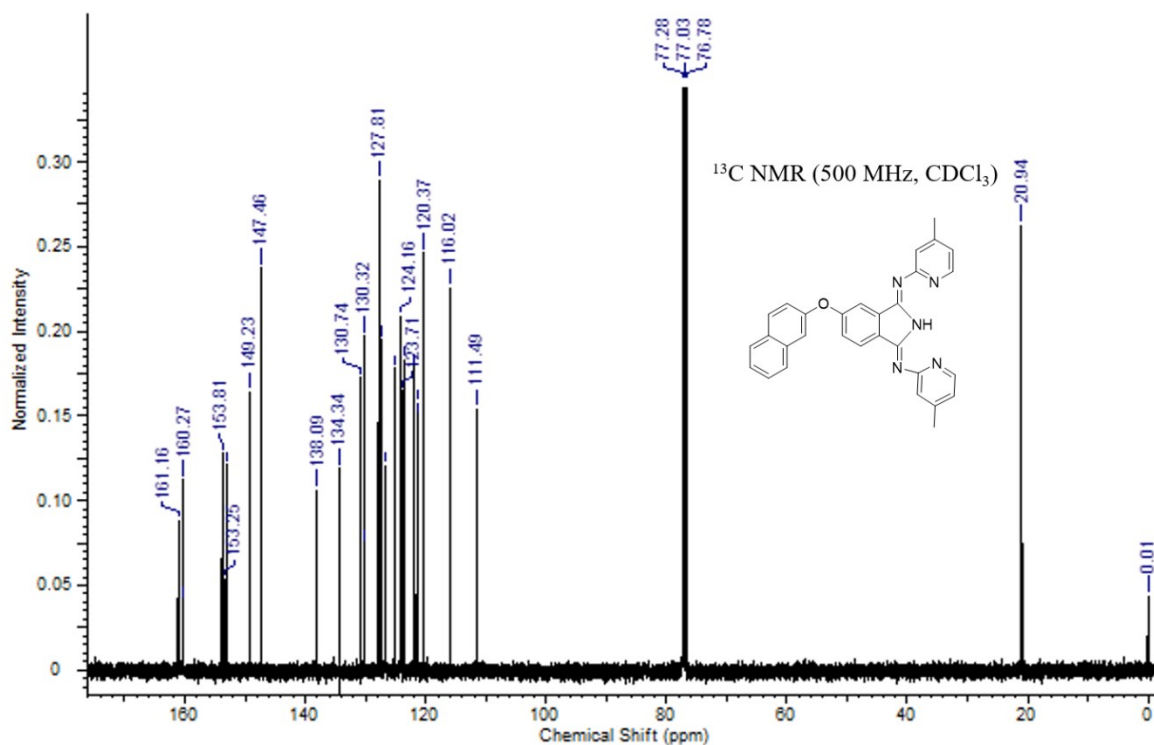


Figure S4. ¹³C-NMR spectrum of BPI in CDCl₃

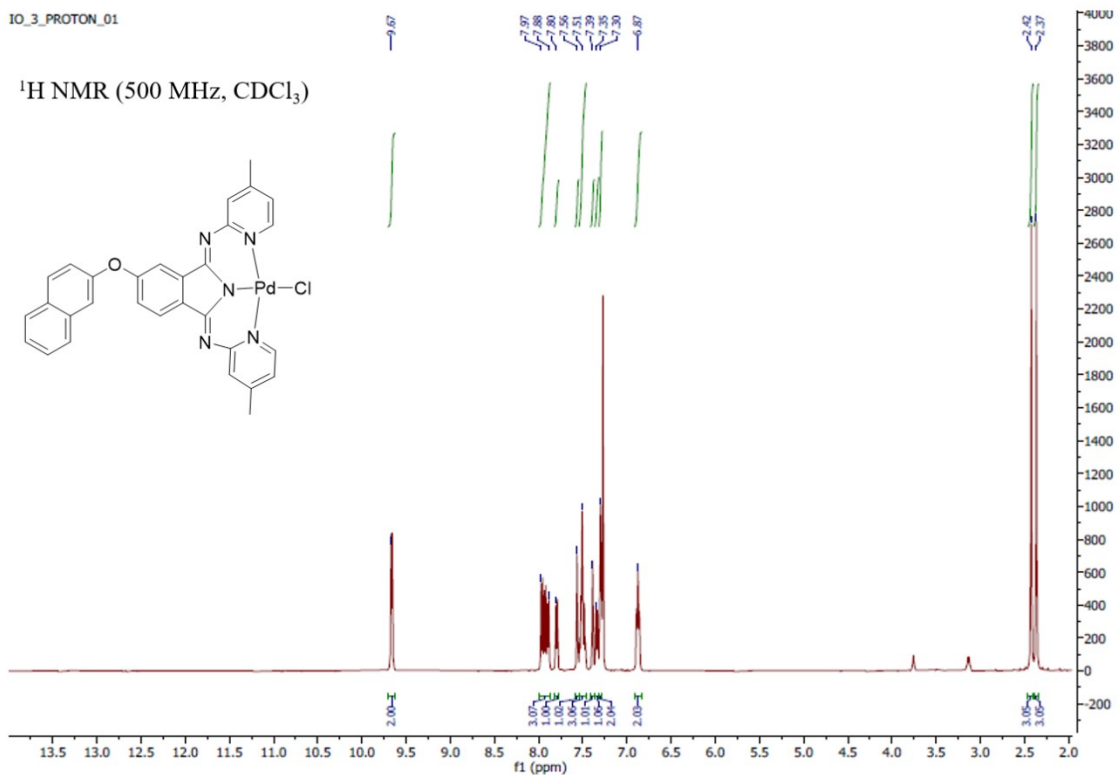


Figure S5. ¹H-NMR spectrum of PdBPI in CDCl₃.

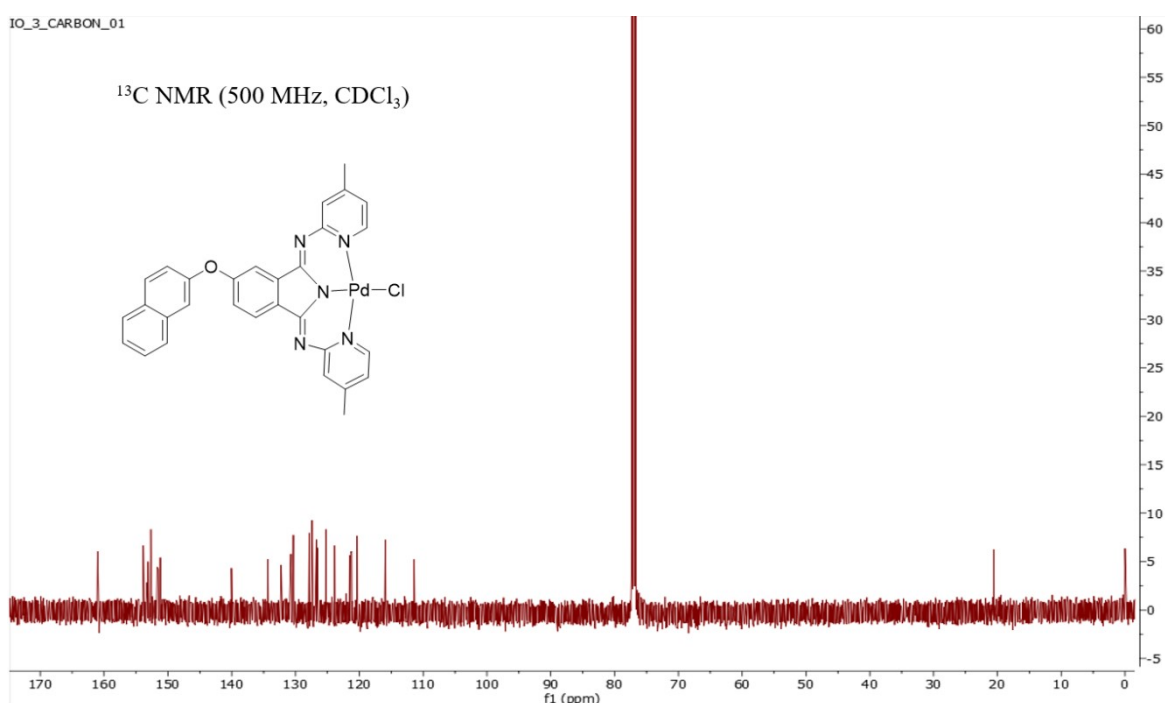


Figure S6. ¹³C-NMR spectrum of PdBPI in CDCl₃

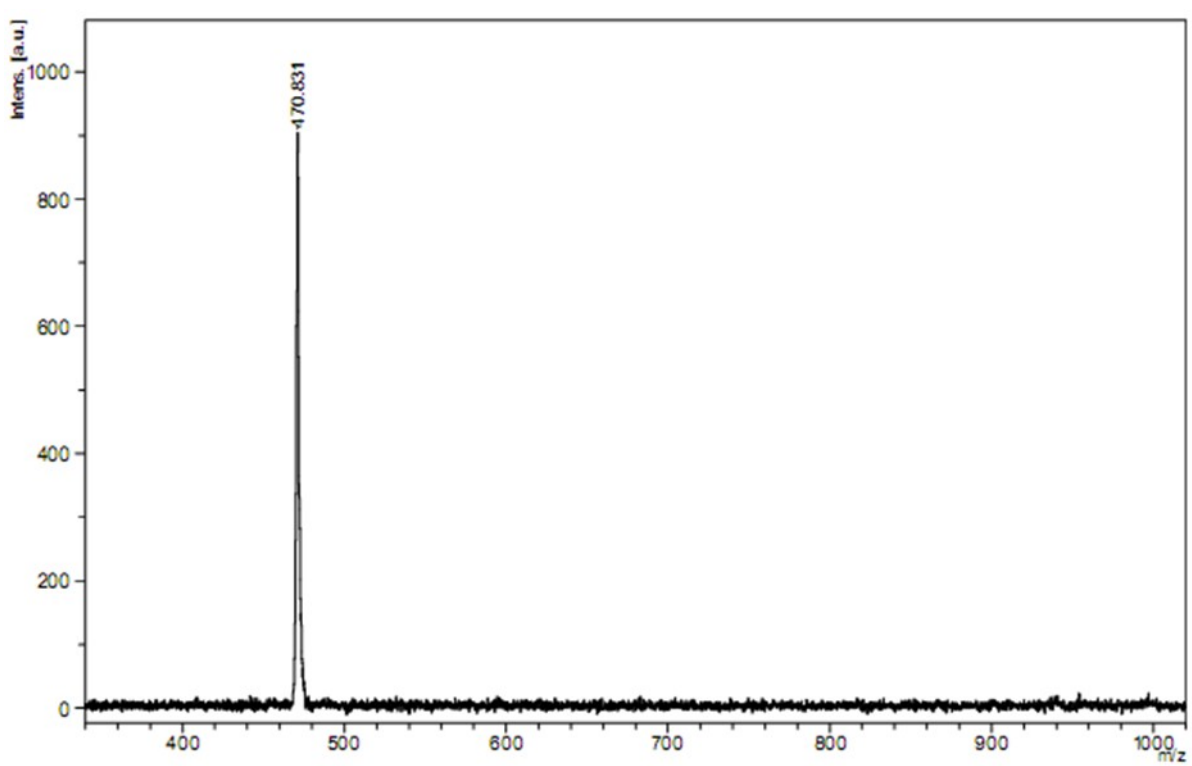


Figure S7. MALDI-TOF MS spectrum of **BPI**.

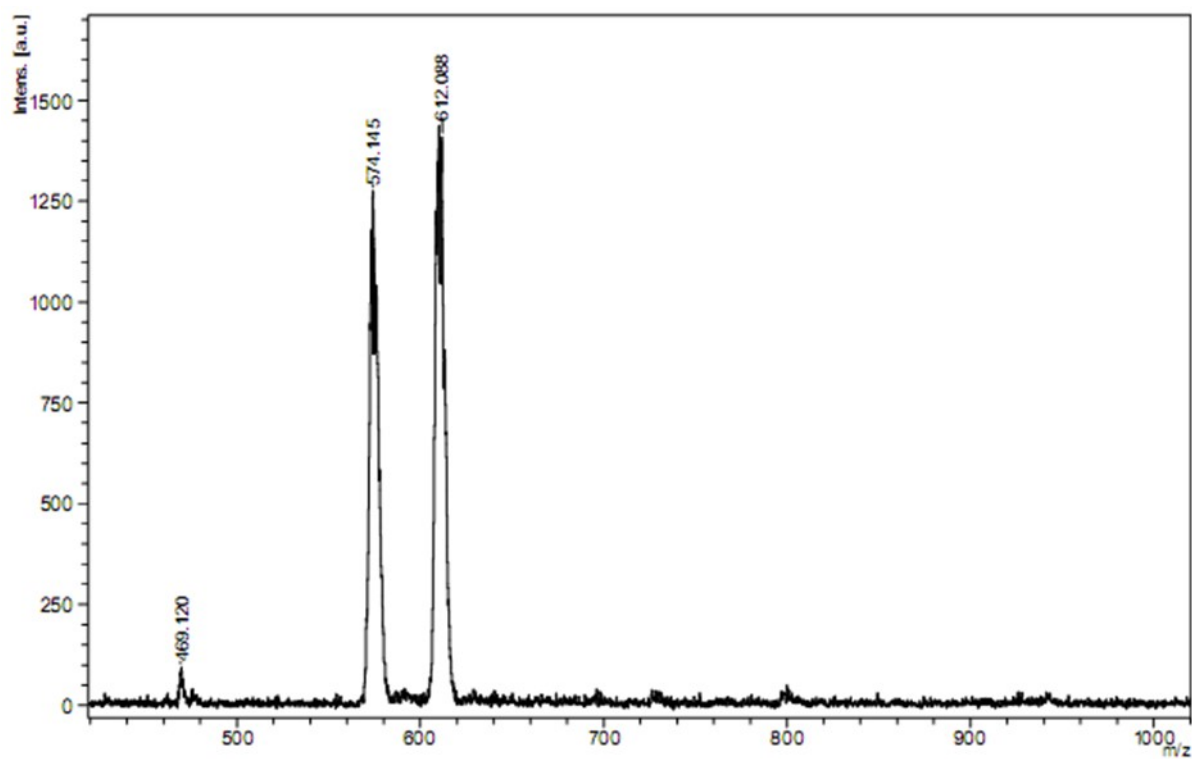


Figure S8. MALDI-TOF MS spectrum of **PdBPI**.

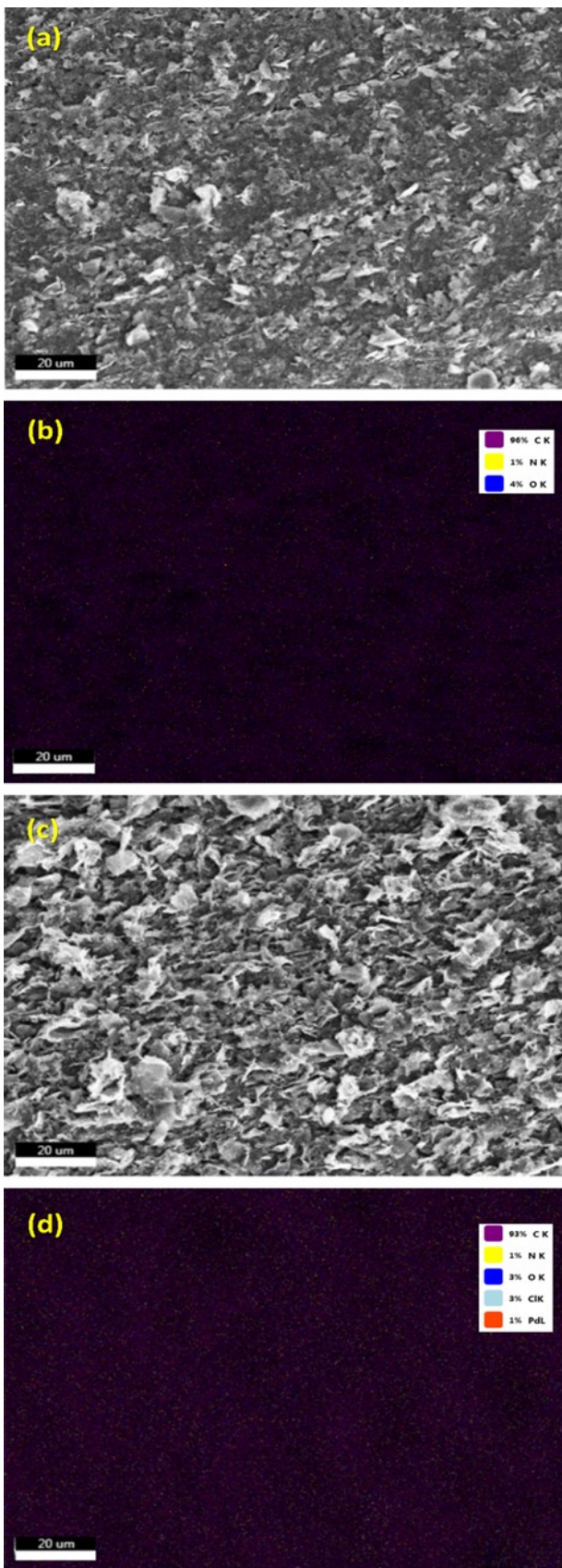


Figure S9. SEM images of PGE/BPI (a) and PGE/PdBPI (c), and EDX elemental mapping results of PGE/BPI (b) and PGE/PdBPI (d).

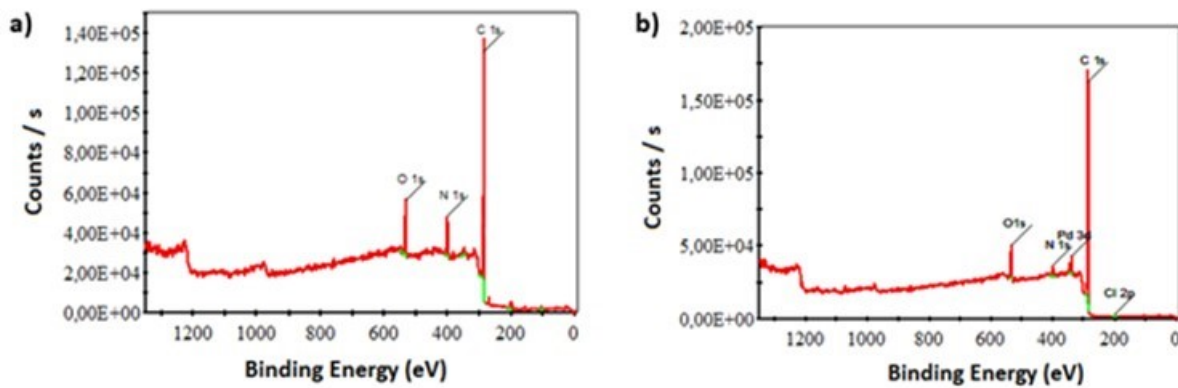


Figure S10. XPS Survey spectra of BPI-CF (a) and PdBPI-CF (b).

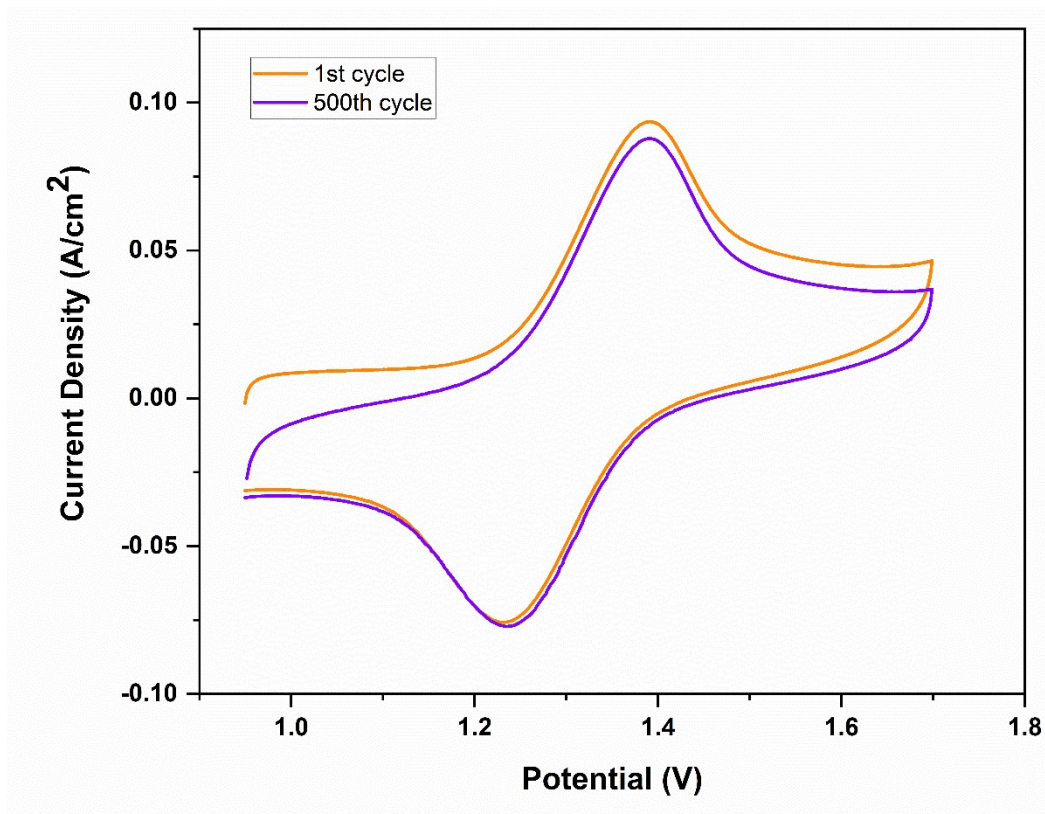


Figure S11. Electrochemical stability test of PGE/BPI.

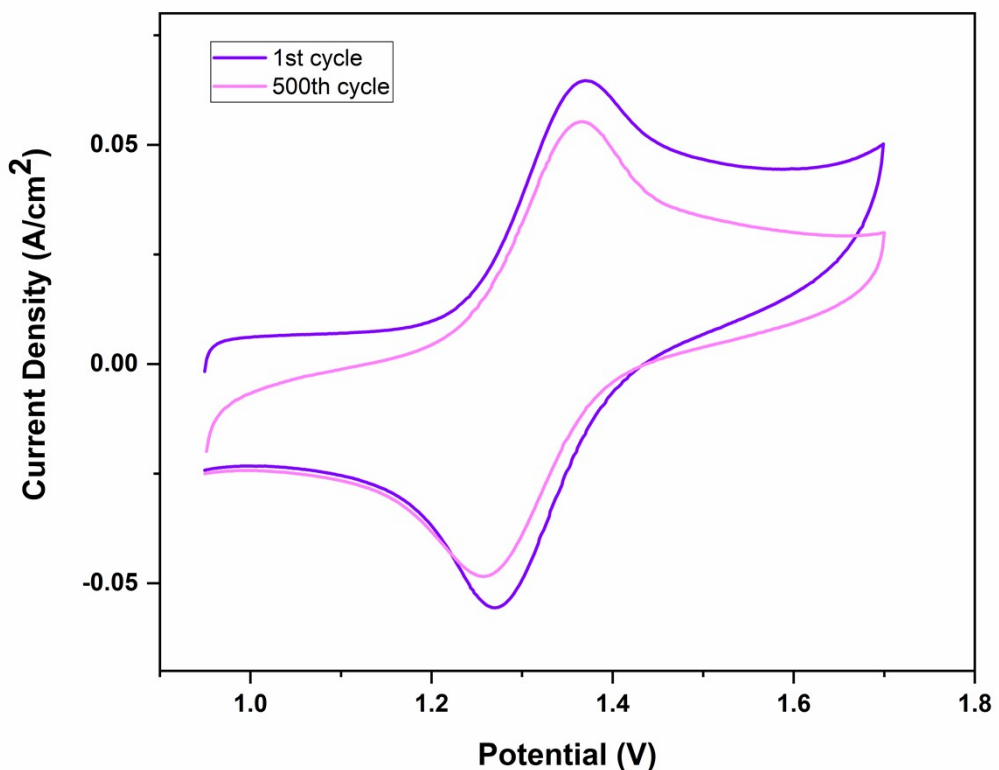


Figure S12. Electrochemical stability test of PGE/PdBPI.

Table S1. Structure refinement parameters of **BPI** and **PdBPI**.

	BPI	PdBPI
Empirical formula	C ₃₀ H ₂₃ N ₅ O	C ₃₀ H ₂₂ ClN ₅ OPd
T(K)	306(0)	303(2)
λ(Å)	0.71073	0.71073
Crystal system	triclinic	triclinic
Space group	P -1	P -1
Unit cell dimensions: (Å, °)		
a	6.3202(3)	8.6324(9)
b	10.3082(5)	10.5581(12)
c	19.4392(9)	16.7354(17)
V(Å³)	1228.62(9)	1412.2(3)
α	82.097(2)	79.298(7)
β	83.015(2)	87.886(7)
γ	79.848(2)	70.496 (7)
Z	2	2
Absorption coefficient (mm⁻¹)	0.080	0.783
D_{calc} (g/cm³)	1.269	1.435
F(000)	492	616
Crystal size (mm)	0.03 x 0.30 x 0.60	0.05 x 0.100 x 0.783
θ range for data collection (°)	2.39 to 25.00	2.22 to 25.00
Index ranges	-7≤h≤7 -12≤k≤12 -23≤l≤23	-10≤h≤10 -12≤k≤12 -19≤l≤19
Reflections collected	51037	20957
Independent reflections	4334	4965
Coverage of independent reflections (%)	99.9	99.6
Data/parameters	4334/327	4965/345
Final R indices [I≥2σ(I)]	R1 = 0.0448 wR2 = 0.111	R1 = 0.0824 wR2 = 0.2033
R indices (all data)	R1 = 0.0715 wR2 = 0.1275	R1 = 0.1901 wR2 = 2409
Goodness-of-fit on F²	1.049	1.097
Largest difference in peak and hole (e Å⁻³)	0.350/-0.140	1.101/-0.739

Table S2. Selected bond lengths (Å) **BPI** and **PdBPI**.

BPI			PdBPI		
N3	H13	0.86	Pd	N1	2.05(1)
H13	N1	2.089	Pd	N3	1.921(8)
N3	C14	1.377(2)	Pd	N5	2.05(1)
C14	N4	1.285(2)	Pd	Cl	2.330(3)
N3	C13	1.379(2)	N3	C14	1.39(1)
C13	N2	1.282(2)	C14	N4	1.28(2)
C6	N1	1.333(3)	N4	C8	1.39(2)
N5	C8	1.344(2)	N3	C13	1.36(2)
C21	O1	1.391(2)	C13	N2	1.28(2)
O1	C20	1.385(2)	N2	C6	1.34(1)
			C6	N1	1.35(2)
			C8	N5	1.34(1)
			C21	O1	1.38(2)
			O1	C20	1.37(1)
			C20	C17	1.40(2)

Table S3. Selected bond angles ($^{\circ}$) **BPI** and **PdBPI**.

C13	N3	C14	113.0(1)	Cl	Pd	N1	91.3(3)
N3	C14	N4	130.0(2)	N3	Pd	N1	88.9(4)
N4	C8	N5	120.6(2)	Cl	Pd	N5	92.8(3)
C21	O1	C20	116.7(1)	N5	Pd	N3	89.7(4)
				N5	C8	N4	125(1)
				N1	C6	N2	124(1)
				C14	N3	C13	108.7(9)

Table S4. Comparison of CE, EE and VE based on previous reported studies.

Material	Coulombic	Energy	Voltage	Ref

	Efficiency (CE) (%)	Efficiency (EE) (%)	Efficiency (VE) (%)	
Phosphonated graphene oxide carbon felt	88.4	80.2	-	1
Graphite felt treated by modified Hummers method (C-OH group)	95.0	77.2	81.3	2
PbO ₂ -modified graphite felt	99.5	82.4	82.0	3
CoTGF	89.5	69.4	77.6	4
HF, H ₂ O ₂ co-modified GF (GF-HF/H ₂ O ₂)	97.3	75.7	77.8	5
GF-H ₂ SO ₄ /GF-G	99.5	95.8	96.3	6
Hydroxylated carbon felt (HCF)	55.0	51.7	94.1	7
Thermal oxidation treatment	95.15	83.18	87.41	8
BPI-CF	86.2	75.1	87.1	In this study
PdBPI-CF	90.4	88.8	98.2	In this study

References

- 1 M. Etesami, E. Abouzari-Lotf, A. Ripin, M. Mahmoud Nasef, T. M. Ting, A. Saharkhiz and A. Ahmad, *Int. J. Hydrogen Energy*, 2018, **43**, 189–197.
- 2 X. Wu, H. Xu, Y. Shen, P. Xu, L. Lu, J. Fu and H. Zhao, *Electrochim. Acta*, 2014, **138**, 264–269.
- 3 X. Wu, H. Xu, L. Lu, H. Zhao, J. Fu, Y. Shen, P. Xu and Y. Dong, *J. Power Sources*, 2014, **250**, 274–278.
- 4 Y. Xiang and W. A. Daoud, *J. Power Sources*, 2019, **416**, 175–183.
- 5 Z. He, Y. Jiang, W. Meng, F. Jiang, H. Zhou, Y. Li, J. Zhu, L. Wang and L. Dai, *Appl. Surf. Sci.*, 2017, **423**, 111–118.
- 6 Z. González, C. Flox, C. Blanco, M. Granda, J. R. Morante, R. Menéndez and R. Santamaría, *J. Power Sources*, 2017, **338**, 155–162.
- 7 M. Zarei-Jelyani, M. Babaiee, A. Ghasemi and R. Eqra, *J. Renew. Energy Environ.*, 2016, **3**, 54–59.
- 8 A. Kaur, K. Il Jeong, S. Su Kim and J. Woo Lim, *Compos. Struct.*, 2022, **290**, 115546.